Contributions to Mineralogy and Petrology (2023) 178:74
https://doi.org/10.1007/s00410-023-02056-2

ORIGINAL PAPER

Petrological and geochemical constraints of mantle peridotites on the magma-starved Yap Arc formed by ultra-slow subduction

Junhua Yao[1,2] · Guoliang Zhang[1,2] · Ji Zhang[1,2] · De-Feng He[3]

Received: 22 January 2023 / Accepted: 9 September 2023 / Published online: 3 October 2023

Abstract

Oceanic plateaus inevitably interact with trench–arc systems during oceanic subduction, but the subduction mechanisms are poorly understood. The Yap trench–arc system is an important part of the western Pacific subduction zone, and is undergoing ultra-slow subduction of the Caroline Plateau. As such, it is ideal for investigating the magmatic–tectonic processes of oceanic plateau subduction. In this study, we document the mineralogy and geochemistry of serpentinized peridotites from the Yap–Mariana Junction. These peridotites can be subdivided into two groups. Group I samples have intermediate to high whole-rock CaO contents and Al_2O_3/SiO_2 values, low chromite Cr# (as low as 0.16) and high chromite Ga/Fe^{3+}# values, and low pyroxene Mg# values relative to Mariana Forearc peridotites. These features are consistent with those of abyssal peridotites. Based on La/Sm ratios, two types of clinopyroxene are identified in group 1 samples. Melting models show that the light rare earth element (LREE)-depleted patterns of type 1 clinopyroxene can be produced by ~ 5% fractional melting or ~ 6% open-system melting of depleted upper mantle, while the nearly flat REE patterns of type 2 clinopyroxene are related to LREE-enriched melts. These clinopyroxene compositions record melt impregnation and reactions in the mantle beneath the Yap–Mariana Junction. In contrast, group 2 samples have similar compositions to forearc peridotites, such as low whole-rock Al_2O_3/SiO_2 values, and high chromite Cr# (up to 0.73) and low chromite Ga/Fe^{3+}# values. The different trends in plots of chromite Cr#–TiO_2 and $100Ti/Fe^{3+}$#–Ga/Fe^{3+}# indicate that the group 1 samples experienced reactions with mid-ocean ridge basalt-like melts, whereas the group 2 samples experienced reactions with island arc tholeiite-like melts. The Mg#, TiO_2, and Al_2O_3 values of the melts in equilibrium with chromite in the group 1 samples are consistent with those of the Parece Vela Basin basalts, while those from group 2 samples define a compositional trend similar to arc-related volcanic rocks. Therefore, this region experienced a tectonic transition from a back-arc spreading ridge to a subduction zone. Compared with the Mariana Trench that is undergoing normal oceanic crustal subduction, the absence of volcanic rocks at the Yap Trench are the response to ultra-slow subduction of the Caroline Plateau.

Keywords Ultra-slow subduction · Oceanic plateau subduction · Mantle peridotites · Mineralogy · Magma-starved Yap Arc

Introduction

Oceanic plateaus cover ~ 3% of Earth's seafloor, and inevitably interact with trench–arc systems during oceanic subduction (e.g., Cloos 1993; Kerr and Mahoney 2007). Compared with normal oceanic crust, oceanic plateaus have anomalously thick crust and a greater buoyancy (Wei et al. 2020). Given that the buoyancy of a subducted slab is the primary driving force for subduction (e.g., Royden and Husson 2009), oceanic plateau subduction can dramatically reduce the subduction rate of a downgoing plate (e.g., Knesel et al. 2008; van Hunen et al. 2002). The subduction rate affects the subduction mechanisms, lithospheric stress state and thermal structure, and nature of volcanism (Gorczyk

Communicated by Timm John.

✉ Guoliang Zhang
zhangguoliang@qdio.ac.cn

[1] Center of Deep Sea Research, Institute of Oceanology, Chinese Academy of Sciences, Qingdao 266071, China

[2] Center for Ocean Mega-Science, Chinese Academy of Sciences, Qingdao 266071, China

[3] State Key Laboratory of Ore Deposit Geochemistry, Institute of Geochemistry, Chinese Academy of Sciences, Guiyang 550081, China

et al. 2007; Holt and Condit 2021; Schellart 2005; Wark et al. 1990). In general, incipient subduction of an oceanic plateau can block a trench and hinder subduction, which causes ultra-slow subduction with a volcanic gap (McGeary et al. 1985). Numerous studies have examined normal oceanic subduction systems with variable subduction rates; e.g., the Tonga (high rate ~ 15 cm/yr), Izu–Bonin–Mariana (IBM; intermediate rate = 3–6 cm/yr), and Andaman (low rate = 2–3 cm/yr) arcs, which has constrained subduction processes, such as the compositional variations of magmatism (forearc basalt–boninite–arc basalt) and release of fluids/melts at different subduction stages (e.g., Doley et al. 2022; Reagan et al. 2010; Stern et al. 2003; Turner et al. 2000). However, in the case of oceanic plateau subduction, previous studies have primarily used geophysical and numerical modeling methods to examine the feasibility of subducting an oceanic plateau and its final fate (e.g., Liu et al. 2021; Nair and Chacko 2008; Rosenbaum et al. 2005). Geochemical constraints on this process are limited, and little is known about the nature of the mantle wedge and associated magmatic–tectonic processes in such ultra-slow subduction systems.

The IBM–Yap trench–arc system is an important part of the western Pacific subduction zone (Fig. 1a), and is a classic example of an intra-oceanic subduction system (e.g., Hawkins et al. 1984; Kobayashi 2004; Stern et al. 2003), with the Yap trench–arc system being a rare case of oceanic plateau subduction (e.g., Fan et al. 2022; Zhang and Zhang 2020). GPS data indicate the Caroline Plateau is subducting at an ultra-low rate (0–6 mm/yr; Seno et al. 1993). A few forearc peridotites (e.g., chromite with Cr# > 60; Chen et al. 2019a, b; Ohara et al. 2002a) and rare arc volcanic rocks (Beccaluva et al. 1986; Crawford et al. 1986) have also been found in the southern and central sections of the Yap Trench. The Yap Trench is directly connected to the Parece Vela Rift to the north, and the northernmost Yap Trench may record the interaction between nascent oceanic crust and the Caroline Plateau, making it an ideal location to study magmatic–tectonic processes during ultra-slow subduction of an oceanic plateau.

In addition to mantle-derived igneous rocks, mantle peridotites can provide information on the deep mantle. Their mineralogical and geochemical characteristics have been widely used to constrain the architecture and composition of the deep mantle and magmatic–tectonic processes (e.g., Arai 1994; Birner et al. 2017; Dick and Bullen 1984; Kamenetsky et al. 2001; Niu 1997, 2004; Ohara and Ishii 1998; Parkinson and Pearce 1998; Warren 2016; Yao et al. 2023). In this paper, we present petrographic, mineral chemistry, and whole-rock major and trace element data for mantle peridotites and metamorphic rock that were recently recovered from the Yap–Mariana Junction. These data constrain the compositional nature and evolution of the upper mantle beneath the Yap–Mariana Junction. Combined with published peridotite data from the Yap Trench, we compared our results with data for peridotites from the Parece Vela Basin (PVB) and Mariana Trench, which provides new insights into the interaction of the Yap Trench with the Caroline Plateau and the mechanisms of ultra-slow subduction.

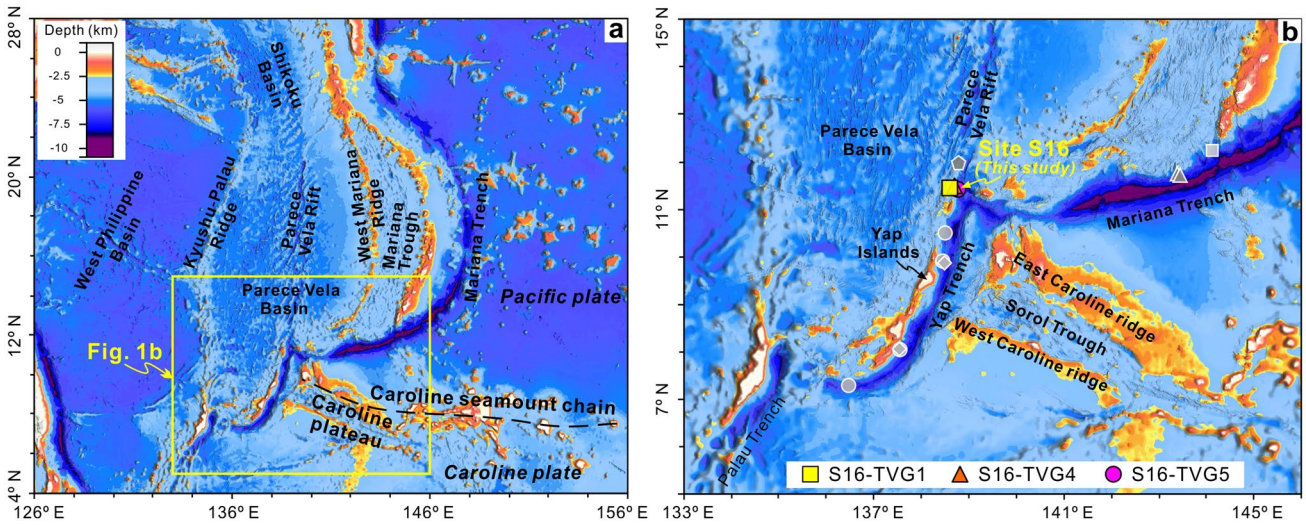

Fig. 1 Bathymetric and tectonic features of the Yap trench–arc system in the western Pacific showing the sampling locations during the R/V *KEXUE* cruise in 2020. The map was produced using GeoMap App software. Data sources of sampling locations for published mantle peridotites: Yap Trench (gray circular: Ohara et al. 2002a, gray rhombus: Chen et al. 2019a, b); Mariana Trench (gray triangle: Ohara and Ishii 1998); Marina Trough (gray square: Michibayashi et al. 2009), Parece Vela Rift (gray pentagon: Gong et al. 2022)

Geological background and sampling

The Yap trench–arc system lies at the southeastern boundary of the Philippine Sea Plate and is a representative example of an oceanic subduction zone (Fig. 1b), where the Pacific and Caroline Plates are subducting beneath the Philippine Sea Plate (Fujiwara et al. 2000; Seno et al. 1993). The ~ 700-km-long Yap Trench has an arcuate shape toward the southeast, a maximum water depth of 8946 m, and is connected with the Parece Vela Rift and Mariana Trench to the north and Palau Trench to the south. It may have been part of the proto-IBM Trench during 40–30 Ma (Kobayashi 2004). However, compared with typical trench–arc systems in the western Pacific (e.g., the Mariana and Japan Trenches), the Yap Trench has some unique characteristics, such as a very short trench–arc distance (~ 50 km; Fujiwara et al. 2000), little intermediate-depth seismicity, and a lack of flat-lying sediments at the trench axis (Dong et al. 2018; Fujiwara et al. 2000) and active arc volcanism (Sato et al. 1997). The Yap Arc consists primarily of greenschists and amphibolites (Hawkins and Batiza 1977). The amphibolites formed at *ca.* 21 Ma, based on amphibole $^{40}Ar/^{39}Ar$ dating and titanite U–Pb dating (Zhang and Zhang 2020). Only two occurrences of island arc volcanic rocks have been reported in the Yap trench–arc system: *ca*. 25 Ma medium-K basalts and basaltic andesites in the North Yap Escarpment (Ohara et al. 2002a) and 10.9–7.6 Ma low-K tholeiites along the landward slope of the Yap Trench (Beccaluva et al. 1986; Crawford et al. 1986). The Caroline Ridge on the Caroline Plate subducted to the northwest and collided with the Yap Trench at *ca*. 21 Ma (Zhang and Zhang 2020), causing an offset of hundreds of kilometers westward from the main IBM trend. The ridge comprises the West and East Caroline Ridges and represents an oceanic plateau formed by a deep-seated hotspot (Zhang et al. 2020).

The PVB is located in the southeastern part of the Philippine Sea Plate, and is an extinct back-arc basin (Karig 1971). It is flanked by the Kyushu–Palau and West Mariana ridges, and is connected to the Shikoku Basin to the north. The PVB started to spread at *ca*. 29 Ma due to slab roll-back along the IBM Trench and had a two-stage rifting history. The first stage comprised E–W rifting during 30–19 Ma (full spreading rate = 88 mm/yr; Okino et al. 1998). The second stage was NW–SE rifting after 19 Ma (full spreading rate = 70 mm/yr; Ohara et al. 2001) in response to clockwise rotation of the Philippine Sea Plate. The spreading ceased at *ca*. 7.9 Ma, based on zircon U–Pb dating of gabbroic and leucocratic rocks from the Godzilla megamullion (Tani et al. 2011). Despite the relatively high/intermediate spreading rate, the PVB contains several megamullions (e.g., the Godzilla Mullion at ~ 16°N; Ohara et al. 2003). Different types of mantle peridotites (e.g., fertile peridotite, dunite, and plagioclase-bearing peridotite) are exposed along the Parece Vela Rift (Ohara et al. 2001, 2003).

The samples examined in this study were collected from the Yap–Mariana Junction using a TV-guided grab (TVG) at Site 16 during the R/V *KEXUE* cruise in 2020 (Fig. 1b). There were three TVG assignments (S16-TVG1, S16-TVG4, and S16-TVG5) that recovered rock samples. The sampling locations are listed in Table S1. Samples of 15 mantle peridotites and 1 metamorphic rock were analyzed, which include 4 serpentinized harzburgites and 1 metamorphic rock (S16-TVG-10) from S16-TVG1, 6 serpentinized dunites/harzburgites from S16-TVG4, and 5 serpentinized lherzolites from S16-TVG5. The peridotite samples are yellowish brown in color, 5–10 cm in size, and have experienced variable seawater alteration. The metamorphic rock is grayish green in color and ~ 5 cm in size. Hand specimens of representative samples are shown in supplementary Figure S1.

Analytical methods

In situ mineral chemistry

The compositions of silicate minerals and chromite/Fe oxides in our samples were determined by wavelength dispersive analysis using a JEOL JXA-8200 electron microprobe at the Institute of Oceanology, Chinese Academy of Sciences (IOCAS), Qingdao, China. The analytical conditions were 15 kV accelerating voltage, 20 nA beam current, 5–10 μm beam diameter, 30 s on-peak counting time, and 15 s off-peak counting time. The ZAF correction method was used to correct for matrix compositional effects. Synthetic oxides and natural minerals were used as standards. The Fe^{2+} and Fe^{3+} contents of chromite and clinopyroxene were calculated from their ideal stoichiometries. Compositional mapping of minerals was undertaken by energy dispersive X-ray spectroscopy using an accelerating voltage of 15 kV and a beam current of 10 nA. The precision of the analysis is better than 3% for major elements (> 1 wt%) and 10% for trace elements (< 1 wt%) which is routinely tested on the standards.

Trace element analyses of clinopyroxene and chromite were conducted by LA–ICP-MS (Laser Ablation Inductively Coupled Plasma Mass Spectrometer) at the State Key Laboratory of Ore Deposit Geochemistry, Institute of Geochemistry, Chinese Academy of Sciences, Guiyang, China, using an Agilent 7700cs quadrupole ICP-MS coupled to a GeoLasPro 193 nm LA system. The detailed operating conditions and analytical procedures were described by Liu et al. (2008) and Pagé and Barnes (2009). Helium was used as a carrier gas

and was mixed with Ar via a T-connector before entering the ICP-MS. The laser beam diameter was 40 µm for chromite and 30 µm for clinopyroxene. Each spot analysis consisted of ~ 30 s of background (gas blank) acquisition followed by 60 s of data acquisition from the sample. Calibration was performed using multiple reference materials (BCR-2G, BIR-1G, BHVO-2G, NIST SRM 610, and NIST SRM 612) combined with internal standardization. ^{29}Si and ^{27}Al were used as internal standards for clinopyroxene and chromite, respectively. Off-line data selection and integration of background and analyte signals, time drift corrections, and quantitative calibrations were undertaken with ICPMSDataCal (Liu et al. 2008). The data for the reference materials are consistent with the recommended values within 10% for most elements.

Whole-rock major and trace elements

Whole-rock major element compositions were determined on fused glass disks by X-ray fluorescence (XRF) spectrometry (ZSX Primus II) at Qingdao Sparta Analysis and Test Company Limited, Qingdao, China. The powdered samples (< 200 mesh) were dried in an oven at 105 °C for 3 h. Loss-on-ignition (LOI) values were measured from the weight lost from the dried sample powder after heating for 2 h at 1000 °C. Then 0.5 g of the dried sample and 5 g of $Li_2B_4O_7$ flux were mixed in an agate mortar, heated in a Pt crucible to 1050 °C, and made into a glass disk used for major element analysis. Certified reference materials (BHVO-2, W-2A, and DTS-2B) were used as standards.

Whole-rock trace element compositions were determined by ICP-MS (Thermo X Series II) at Guizhou Tongwei Analytical Technology, Guiyang, China. The powdered samples (50 mg) were dissolved in 2 mL of HF and 1 mL of HNO_3 in closed Teflon beakers at 100 °C for 24 h. The beakers were placed on a hotplate, and the solutions were evaporated to dryness. Subsequently, 1 mL of HNO_3 and 2 mL of HF were added, and the sample solutions were placed in a digestion bomb (i.e., a Teflon capsule and stainless steel bomb jacket). The sealed bombs were heated in an electric oven at 185 °C for 72 h. After cooling, the bombs were opened, and the solutions were evaporated to dryness on a hotplate at 110 °C. This was followed by the addition of 2 mL of HNO_3, before the sample was dried down to convert the residual solids into nitrates. The final residues were dissolved in 3 mL of 2N HNO_3 in the bombs at 130 °C for 12 h. Internal standards of 10 ppb ^{61}Ni and 6 ppb In, Rh, and Re were used to monitor signal drift during analysis. The solutions were diluted by a factor of 4000 times with 1% distilled HNO_3 prior to analysis. The standard solutions (American Lab Tech Company) were diluted to 1, 10, 50, 100, and 400 µg/L to produce calibration curves with linear regression coefficients of > 0.9999. International reference standards (BHVO-2, W-2A, and DTS-2B) were analyzed as unknowns, and our measured values are within uncertainties of the recommended values (http://georem.mpch-mainz.gwdg.de/).

Results

Petrography

Our mantle peridotite samples from the Yap–Mariana Junction have undergone severe serpentinization (> 70%), the extent of which increases generally from fertile to depleted peridotites. Olivines in all samples have been completely altered to pseudomorphic, mesh-textured serpentine, whereas relict orthopyroxene (Opx) and clinopyroxene (Cpx) are occasionally preserved in the serpentinized harzburgites and lherzolites (Fig. 2). Opx and Cpx have coarse-grained or porphyroclastic textures (Fig. 2a, b). Exsolution lamellae of clinopyroxene are common in orthopyroxene (Fig. 2c). Amphibole occurs as replacement rims around clinopyroxene or as discrete porphyroclastic grains in all samples (Fig. 2d). Chromite with an irregular shape and dark reddish brown color is the only primary mineral in all peridotite samples, and is replaced by magnetite and ferritchromite along grain rims or cracks (Fig. 2e). Different types of serpentinized peridotites exhibit several specific petrographic features. For example, in the S16-TVG1 harzburgites, Cpx occurs as two types: (1) anhedral clinopyroxene that is tens of microns in size hosted in Opx (Fig. 2a); and (2) subhedral clinopyroxene that is hundreds of microns in size (Fig. 2b). Micron-sized magnetite occurs as vein-like granular aggregates (Fig. 2e). One grain of platy phlogopite was identified that is ~ 200 µm in length and ~ 100 µm in width (Fig. 2f). In the S16-TVG4 dunites, there are some spongy textured chromite grains with primary cores and porous rims. The rims are Fe-rich and Al-poor relative to the cores (Figure S2a). Multiple serpentine veins crosscut the earlier serpentine mesh texture that replaced olivine and orthopyroxene (Fig. 2g), indicating these samples experienced multiple stages of serpentinization. In the S16-TVG5 lherzolites, Cpx is more abundant and larger (hundreds of microns to millimeters) than in the other peridotite samples. Coarse-grained Cpx is variably altered into serpentine or amphibole along its margins and cleavage (Figs. 2h, i and S2b). The clinopyroxenes can be divided into two groups: type 1 Cpx (low La/Sm) and type 2 Cpx (high La/Sm). A few small orthopyroxene and clinopyroxene inclusions occur as paragenetic aggregates in chromites in the serpentinized lherzolites (Fig. 2j). Moreover, some sheared Opx grains (Fig. 2k) and a pervasive porphyroclastic texture are evidence of weak deformation.

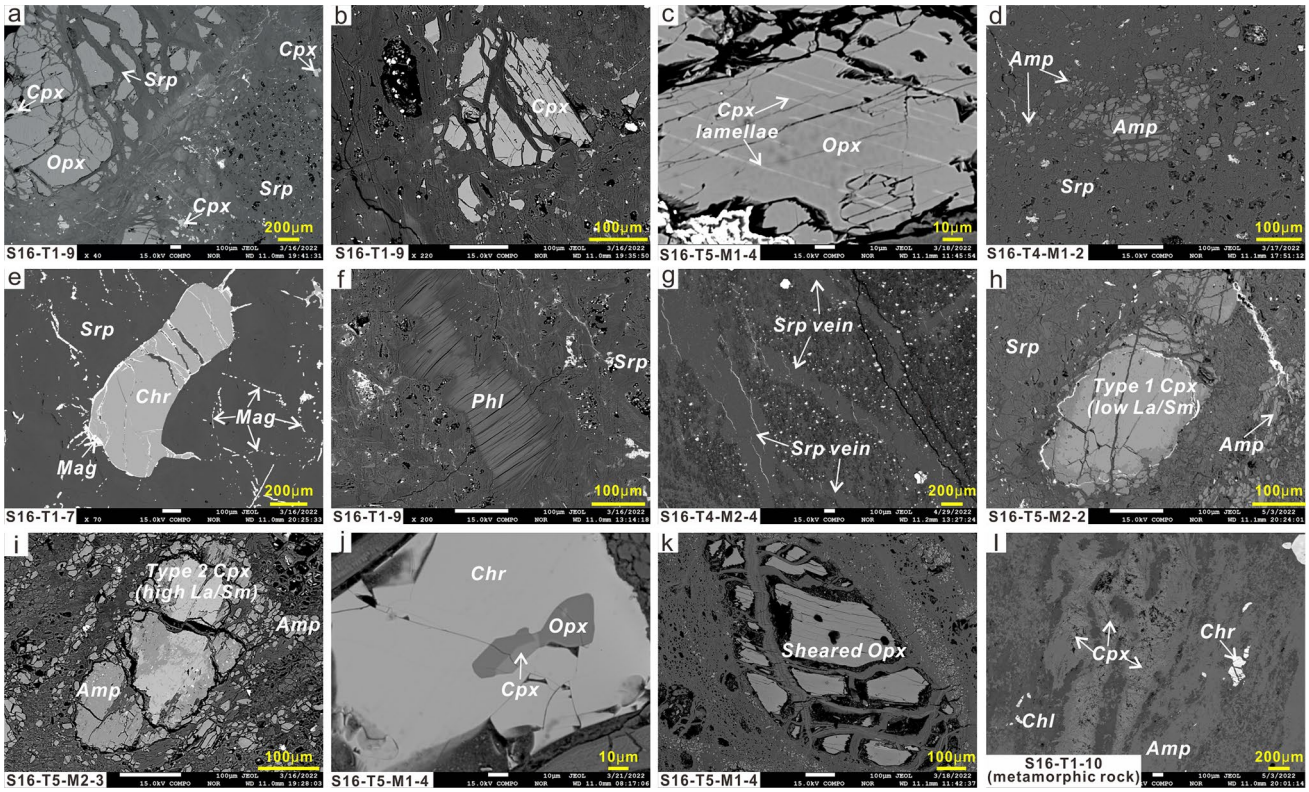

Fig. 2 Back-scattered electron images of mineral assemblages in the different types of samples (serpentinized peridotites and a metamorphic rock) from the Yap–Mariana Junction. Amp = amphibole, Chl = chlorite, Chr = chromite, Cpx = clinopyroxene, Opx = orthopyroxene, Phl = phlogopite, Srp = serpentine, and Mag = magnetite

The metamorphic rock (S16-T1-10) comprises amphibole and chlorite, with minor clinopyroxene and chromite (Fig. 2l), indicative of greenschist-facies metamorphism. It has a weak foliation defined by the alignment of mineral aggregates. Amphibole occurs mainly as slender, needle-like crystals that are a few microns in size and forms aggregates that are intergrown with chlorite, or occasionally as coarser grained crystals that are hundreds of microns in size. Chlorite is much less common than amphibole. Clinopyroxene that is < 10 μm in size occurs as aggregates and is rimmed by actinolite. In contrast to the serpentinized peridotites, chromites in the metamorphic rock are subhedral–anhedral, ellipsoidal or rhombic in shape, and tens to hundreds of microns in size.

Mineral chemistry

Major element compositions of minerals in the serpentinized peridotites and metamorphic rock are presented in Table S2. Microprobe analysis of the chromite focused mainly on the unaltered parts of grains. In the serpentinized peridotites, chromites from S16-TVG4 have a relatively depleted composition, with Cr# = 0.52–0.73 [molar Cr/(Cr + Al)], Mg# = 0.32–0.54 [molar Mg/(Mg + Fe^{2+})], Fe^{3+}# = 0.05–0.12 [molar Fe^{3+}/(Cr + Al + Fe^{3+})], and 0.1–0.4 wt.% TiO_2 (Fig. 3). Chromites from S16-TVG5 have relatively enriched compositions, with Cr# = 0.15–0.29, Mg# = 0.61–0.75, Fe^{3+}# = 0.01–0.04, and 0.02–0.14 wt% TiO_2. Chromites from S16-TVG1 have intermediate compositions, with Cr# = 0.34–0.41 and Mg# = 0.51–0.71. Chromites from the metamorphic rock (S16-T1-10) have high TiO_2 (0.7–1.0 wt%) and intermediate Al_2O_3 (18.4–25.5 wt%) contents.

Unaltered relict pyroxenes occur in the serpentinized harzburgites (S16-TVG1), lherzolites (S16-TVG5), and metamorphic rock (S16-T1-10). Clinopyroxenes from the serpentinized peridotites have a diopsidic composition (Figure S3a), with Mg# = 0.91–0.94 [molar Mg/(Mg + Fe^{Total})], 1.4–5.3 wt% Al_2O_3, 0.2–1.4 wt% Cr_2O_3, and 21.2–25.2 wt% CaO (Fig. 4). Orthopyroxenes are mainly enstatite to pigeonite (Figure S3a), with Mg# = 0.90–0.91, 0.4–4.1 wt% CaO, and 4.8–6.2 wt% Al_2O_3 (Fig. 5). Clinopyroxenes from the metamorphic rock have a composition similar to augite, with low Mg# (< 0.9), Al_2O_3 (< 1 wt%), and Cr_2O_3 (close to zero) values. The compositions of pyroxenes in the serpentinized peridotites from the Yap–Mariana Junction are similar to those from the PVB and plot within the compositional field of abyssal peridotites, but less depleted relative to those

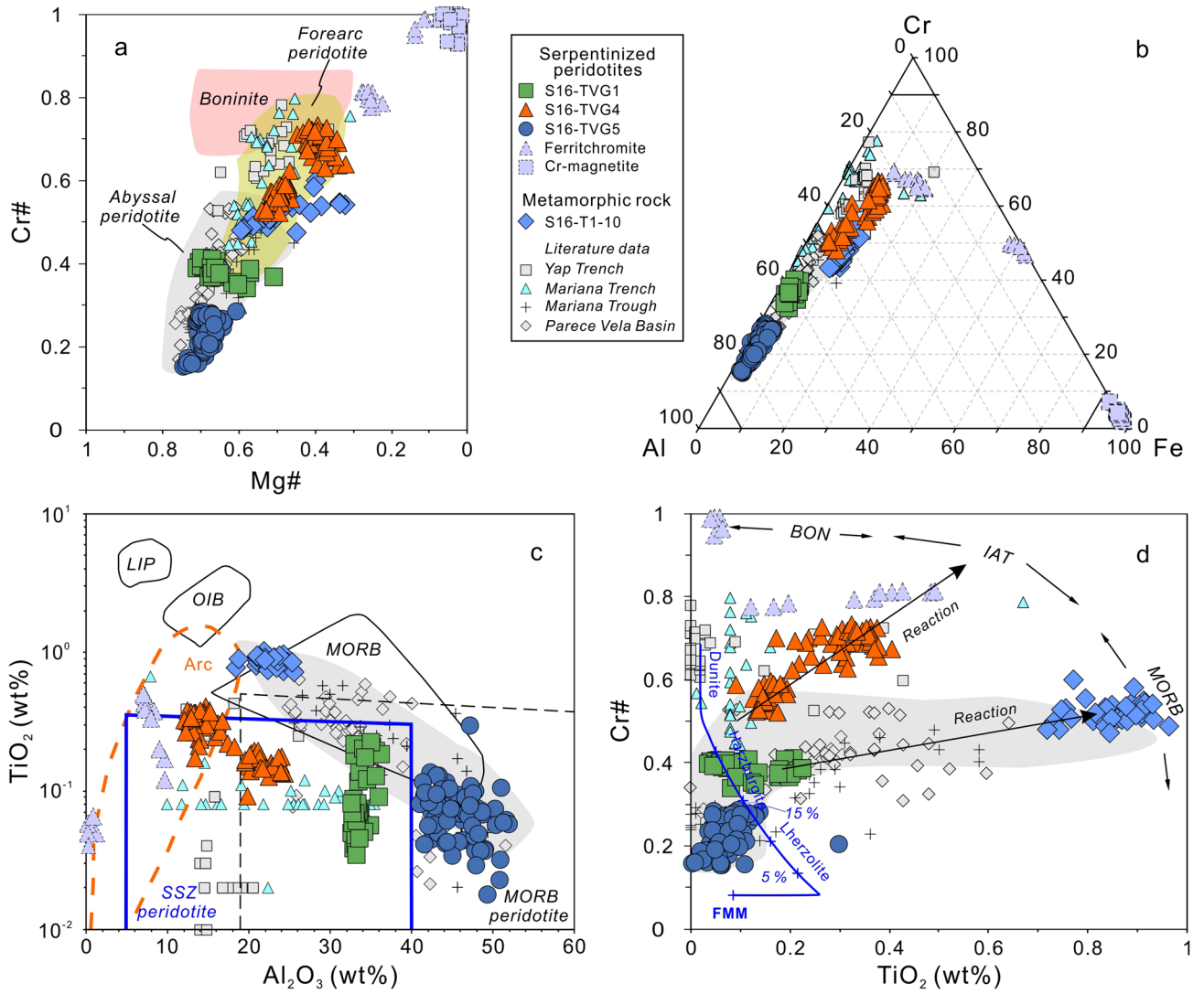

Fig. 3 Plots of chromite **a** Cr# versus Mg#, **b** Cr–Al–Fe^{3+}, **c** TiO_2 versus Al_2O_3, and **d** Cr# versus TiO_2. Fields in (**a**) and (**c**) are after Kamenetsky et al. (2001) and Tamura and Arai (2006); fields in (**d**) are after Tamura and Arai (2006). Fertile MORB mantle (FMM) is from Arai (1994). *MORB* mid-ocean ridge basalt, *SSZ* supra-subduction zone, *LIP* large igneous province basalt, *OIB* ocean island basalt, *Arc* arc-related rock, *BON* boninite, and *IAT* island arc tholeiite. Data sources: Yap Trench (Chen et al. 2019a; Ohara et al. 2002a); Mariana Trench (Ohara and Ishii 1998; Parkinson and Pearce 1998); Mariana Trough (Michibayashi et al. 2009; Ohara et al. 2002b); Parece Vela Basin (Gong et al. 2022; Loocke et al. 2013; Ohara et al. 2003); Abyssal peridotite (Dick and Bullen 1984; Standish et al. 2002)

from the Mariana Trench, with the former having relatively high CaO and Cr_2O_3 contents and low Mg# values (Figs. 4, 5). Chromite-hosted orthopyroxene and clinopyroxene inclusions are enstatite and diopside, respectively, and similar to the unaltered pyroxenes in the samples.

Amphiboles are abundant in these samples and exhibit a wide compositional variation (Figure S3b). Amphiboles from the serpentinized harzburgites (S16-TVG1) are tremolite, while those in the serpentinized dunites (S16-TVG4) and lherzolites (S16-TVG5) are tremolite–edenite and hornblende–pargasite with increasing Si and Na + K contents, respectively. Such compositional variations have also been reported for serpentinized peridotites from the PVB (Gong et al. 2022; Ohara et al. 2003; Sen et al. 2021) and Mariana Trench (Parkinson and Pearce 1998). Amphiboles from the metamorphic rock have hornblende compositions.

Phlogopite in the S16-T1-9 sample has 40.1–41.7 wt% SiO_2, 23.9–25.9 wt% MgO, 8.5–13.1 wt% K_2O, and 1.3–1.6 wt% Cr_2O_3. Similarly, a small amount of phlogopite occurs in plagioclase-bearing peridotites from the PVB (Ohara et al. 2003) and serpentinized dunites from the IBM Trench (Parkinson and Pearce 1998), which is considered to have formed by late-stage, high-temperature seawater circulation rather than by melt–mantle interactions.

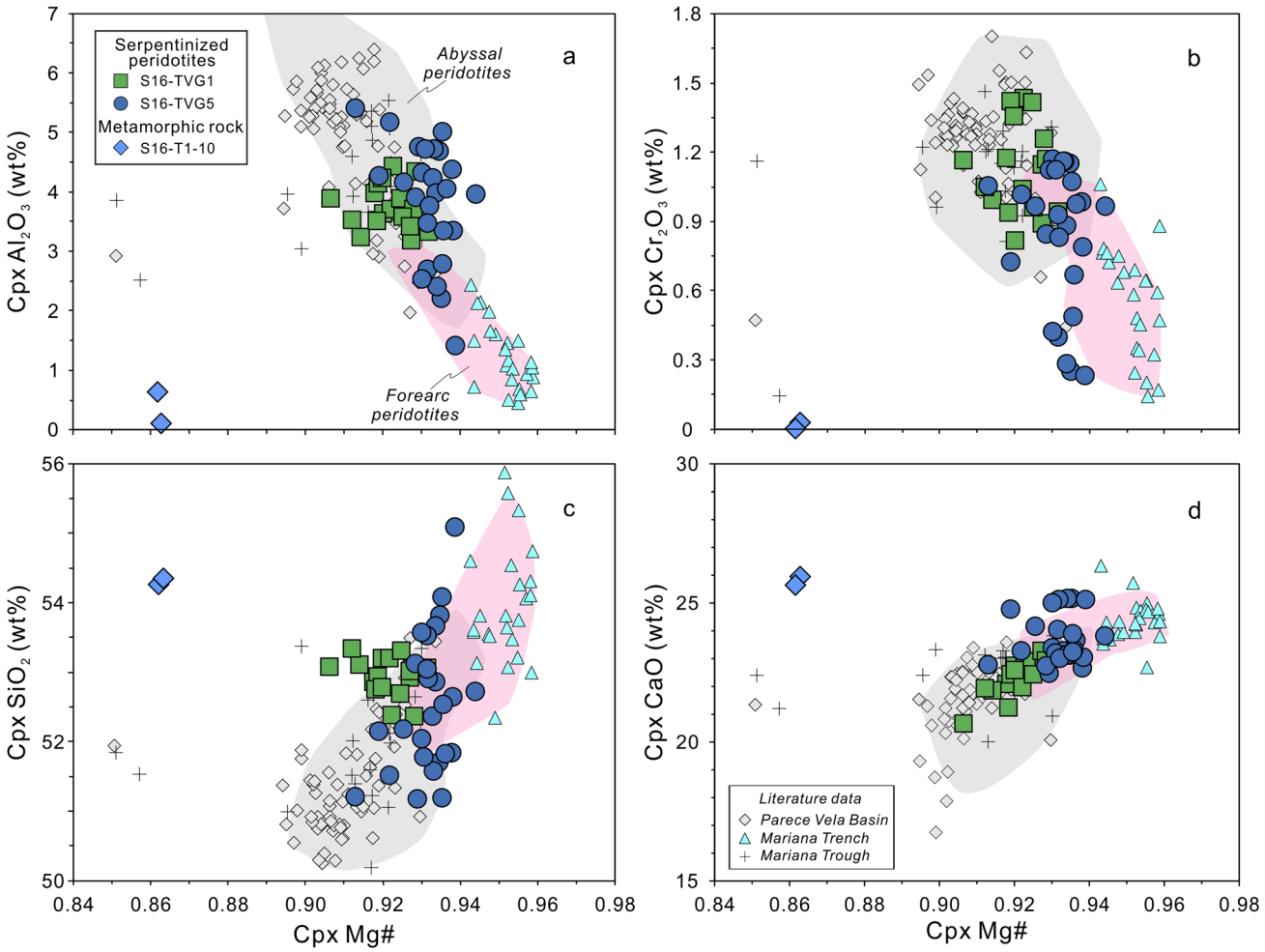

Fig. 4 Major element compositions of clinopyroxene in the serpentinized peridotites and metamorphic rock from the Yap–Mariana Junction. Mg# versus **a** Al_2O_3, **b** Cr_2O_3, **c** SiO_2, and **d** CaO. Data for the abyssal peridotites field are from Warren (2016). Data for the forearc peridotites field are from Birner et al. (2017), Murata et al. (2009), Okamura et al. (2006), Parkinson and Pearce (1998), and Zanetti et al. (2006). Sources of other data are as in Fig. 3

The chromite has Sc contents of ~ 0.5 ppm (S16-TVG5; 0.47–0.60 ppm) to a few parts per million (S16-TVG4; 1.5–5.8 ppm) (Table S3; Figure S4). Chromites in the serpentinized peridotites and metamorphic rock from S16-TVG1 have higher V and lower Co and Zn contents (1130–1410 ppm V; 280–410 ppm Co; 1140–2320 ppm Zn) than those of S16-TVG4 and S16-TVG5 (610–960 ppm V; 450–550 ppm Co; 2010–2890 ppm Zn). The Cr# values of chromite in our samples exhibit a positive correlation with Mn contents and negative correlations with Ni, Ga, and V/Sc values (Figure S4).

Trace element data for clinopyroxene from the S16-TVG5 serpentinized peridotites are listed in Table S4. Although there is no obvious difference in the major element composition and texture, the light rare earth element (LREE) contents of the clinopyroxenes define two types: type 1 Cpx (low La/Sm ratios of 0.02–0.30) and type 2 Cpx (high La/Sm ratios of 0.92–0.96). In chondrite-normalized REE patterns (Fig. 6a), type 1 Cpx exhibits moderate LREE depletion, whereas type 2 Cpx has less-depleted LREE contents and similar middle (M)–heavy (H)REE contents, nearly flat REE patterns, and slightly negative Eu anomalies.

Whole-rock major and trace elements

All the peridotite samples have high LOI values of 11.9–16.8 wt% (Table S5) that gradually increase from the serpentinized lherzolites (S16-TVG5) through to the serpentinized harzburgites (S16-TVG1) and serpentinized dunites (S16-TVG4). Major element contents of these samples have less-depleted compositions relative to Mariana Forearc peridotites, with relatively low MgO/SiO_2 (0.68–0.97) and high Al_2O_3/SiO_2 (0.01–0.07), SiO_2 (43.5–47.7 wt%), Al_2O_3 (0.5–3.0 wt%), and Na_2O (0.15–0.85 wt%) values (Figs. 7

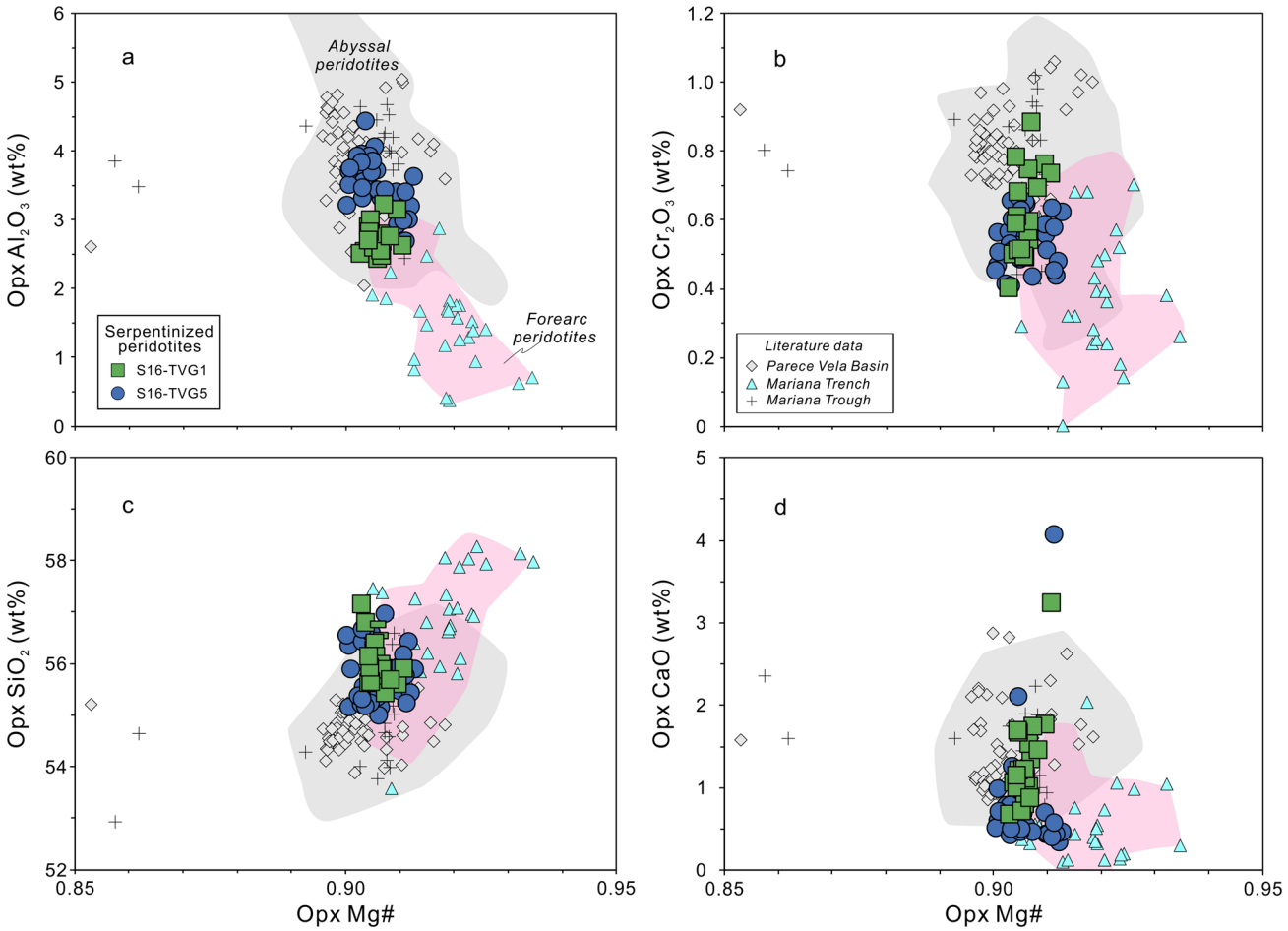

Fig. 5 Major element compositions of orthopyroxene in the serpentinized peridotites from the Yap–Mariana Junction. Mg# versus **a** Al_2O_3, **b** Cr_2O_3, **c** SiO_2, and **d** CaO. Data sources are as in Fig. 4

and S5a–f). The high and variable contents of Ni, V, and Cr (Figure S5g–i) imply that their protoliths contained large amounts, but varying proportions, of olivine, pyroxene, and chromite. The metamorphic rock contains 26.3 wt% MgO, 44.5 wt% SiO_2, 11.8 wt% Al_2O_3, and 7.9 wt% CaO.

Whole-rock chondrite-normalized REE and primitive-mantle-normalized trace element patterns for our samples are presented in Figure S6. All peridotites from the Yap–Mariana Junction exhibit weak LREE enrichment relative to the MREEs [$(La/Sm)_N = 1.46–2.74$, where the subscript N denotes the chondrite-normalized concentration] and have higher REE contents than the Mariana Forearc peridotites (Figure S6a). Most S16-TVG4 and S16-TVG5 samples have negative Ce anomalies relative to La and Pr. A positive Eu anomaly characterizes a serpentinized harzburgite sample (S16-T1-3). The metamorphic rock exhibits moderate LREE enrichment and positive Ce and Eu anomalies. In contrast to the strong enrichment of large-ion lithophile elements in the Mariana Forearc peridotites, our samples have relatively flat primitive-mantle-normalized trace element patterns, with evidence of seawater alteration, such as prominent enrichment in U, Pb, P, and Li relative to adjacent elements (Figure S6b).

Discussion

Protoliths of the serpentinized peridotites and metamorphic rock

For the serpentinized peridotites from the Yap–Mariana Junction, the wide range of whole-rock Al_2O_3 contents from 0.5 to 3.0 wt%, CaO contents from 0.01 to 3.9 wt%, and Al_2O_3/SiO_2 ratios from 0.01 to 0.07 indicate their protoliths varied from fertile to depleted peridotites. In a plot of whole-rock MgO/SiO_2 versus Al_2O_3/SiO_2 (Fig. 7), the Yap serpentinized peridotites have lower MgO/SiO_2 ratios than the terrestrial array (i.e., the trend formed by successive melt extraction from primitive mantle), which is probably related to the loss of MgO during seafloor weathering (Snow

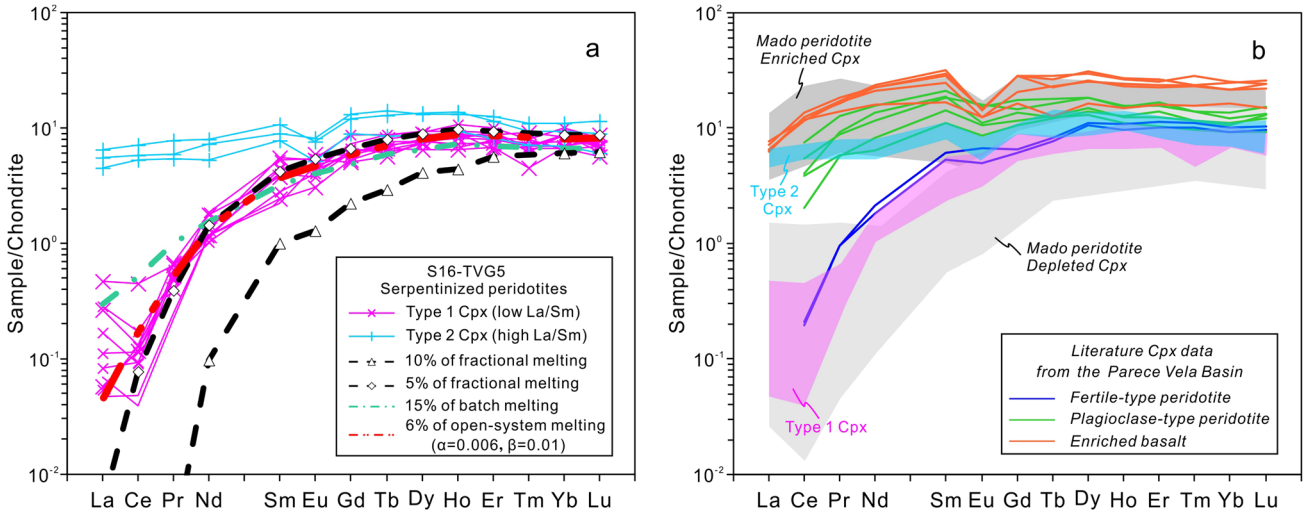

Fig. 6 **a** Chondrite-normalized REE patterns of the two types of clinopyroxene (type 1 with low La/Sm ratios and type 2 with high La/Sm ratios) in the serpentinized peridotites from S16-TVG5. The dashed lines denote the compositions of residual clinopyroxenes produced by batch, fractional, and open-system melting processes from depleted MORB mantle. The fractional melting model with $F=5\%$ (F = degree of partial melting) and open-system melting model with $\alpha=0.006$ (α = melt porosity), $\beta=0.01$ (β = enriched melt influx rate), and $F=6\%$ are in good agreement with the REE data for type 1 clinopyroxene. **b** Comparison of our reported clinopyroxene composition with those in the different types of peridotites (Ohara et al. 2003) and enriched basalts (Yuan and Yan 2022) from the PVB and two types of clinopyroxene in the Mado peridotites from the Shikoku Basin (Sen et al. 2021). The normalizing values for chondrite are from Boynton (1984)

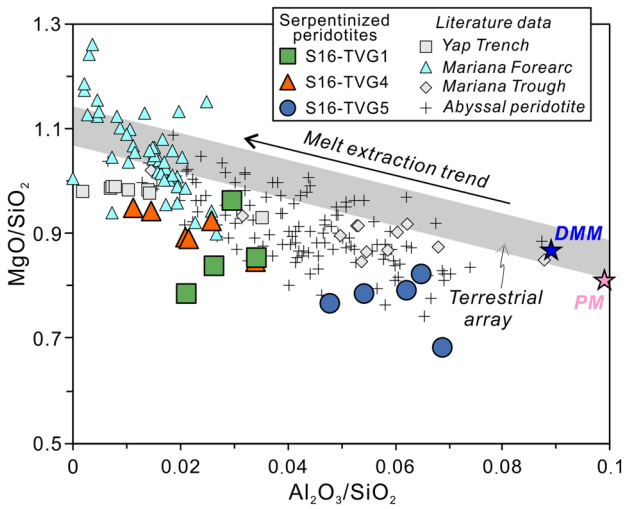

Fig. 7 Plot of whole-rock Al_2O_3/SiO_2 versus MgO/SiO_2. The gray field represents the terrestrial array (Jagoutz et al. 1979). PM (primitive mantle) and DMM are from Palme and O'Neill (2003) and Workman and Hart (2005), respectively. Data sources: Yap Trench (Chen et al. 2019a, b), Mariana Forearc (Parkinson and Pearce 1998; Saboda et al. 1992), Mariana Trough (Michibayashi et al. 2009), and abyssal peridotite (Niu 2004). All whole-rock compositions (including the literature data) were normalized to 100% anhydrous silicate compositions

and Dick 1995) or serpentinization (~ 10% relative MgO loss; Niu 2004). The S16-TVG1 and S16-TVG5 peridotite samples plot in the field for abyssal peridotites, while the S16-TVG4 samples plot in the overlapping area of abyssal peridotites and Mariana Forearc peridotites. This indicates these serpentinized peridotites were derived from two different tectonic environments. However, all the peridotites have undergone severe seawater alteration and the metamorphic rock has experienced greenschist-facies metamorphism. The study area is located in a complex tectonic belt that is a triple junction consisting of the Yap Trench, Mariana Trench, and Parece Vale back-arc spreading ridge. Determining the protolith prior to serpentinization or metasomatism is needed to better constrain the origin and tectonic setting of these samples.

Given that seawater alteration and serpentinization affect whole-rock major and trace element compositions, unaltered minerals are a better means to determine the nature of the protoliths. The samples contain unaltered chromites and minor relict pyroxenes. Previous studies have suggested that the major and trace element compositions of chromite can be used to identify the magmatic processes and tectonic setting of mantle peridotites, chromite deposits, and igneous rocks (e.g., Dick and Bullen 1984; Kamenetsky et al. 2001; Pagé and Barnes 2009; Yao et al. 2018, 2019; Zaccarini et al. 2011). As shown in Fig. 3a and c, the low Cr# and TiO_2, and high Mg# and Al_2O_3 values of chromites in the S16-TVG1 and S16-TVG5 serpentinized peridotites are

similar to those of the PVB (Ohara et al. 2003) and Mariana Trough (Ohara et al. 2002b), and plot in the field for abyssal peridotites (Dick and Bullen 1984). In comparison, chromites in the S16-TVG4 samples have higher Cr# and lower Al_2O_3 and Mg# values relative to the former, and plot in the forearc (i.e., supra-subduction zone [SSZ]) peridotite field. The high TiO_2 and moderate Al_2O_3 contents of chromite in the metamorphic rock are different from those of arc basalt, large igneous province (LIP), ocean island basalt (OIB), and mid-ocean ridge peridotite, but resemble those of mid-ocean ridge basalt (MORB). Moreover, as shown in Fig. 3d, TiO_2 contents of chromites in the S16-TVG4 samples exhibit a wide range and are positively correlated with Cr# values. This is indicative of melt–rock reactions between dunite and an island arc tholeiitic (IAT) melt, which is different from the Mariana Trench. In contrast, chromite data from the PVB and Mariana Trough, and Cr# and TiO_2 values of chromite in the S16-TVG1 and S16-TVG5 peridotites and metamorphic rock plot on the melt–rock reaction trend between lherzolite/harzburgite and a MORB-like melt.

Selected chromite major and trace elements were normalized to the composition of MORB chromite and presented in a multi-element diagram as proposed by Pagé and Barnes (2009). Unaltered chromites from the S16-TVG1 and S16-TVG5 serpentinized peridotites have relatively flat patterns from Al to Mn, with negative Ti and Sc anomalies and positive Zn anomalies (Fig. 8a). A similar MORB-normalized pattern for chromite was reported for high-Al chromitite from the Cerro Colorado ophiolite that formed in a back-arc basin environment (Mendi et al. 2020). The MORB-normalized patterns of the S16-TVG4 chromites exhibit slightly positive slopes from Al to Mn, with positive Ti and Mn anomalies and variable Sc contents (Fig. 8b), which are similar to those of boninitic lavas and high-Cr chromitites from the Thetford Mines Ophiolite (TMO) in Canada (Pagé and Barnes 2009). Compared with the serpentinized peridotites, a positive Ti anomaly is the most significant feature of the chromites in the metamorphic rock (Fig. 8c), as also reported for the Jinchuan mafic–ultramafic igneous rocks (Kang et al. 2022) and Hawaiian tholeiites (Pagé et al. 2011). Given that Ga and Fe^{3+} have similar ionic radii but only Fe^{3+} is redox dependent, the chromite Ga/Fe^{3+}# ratio is largely unaffected by magmatic differentiation. The Ti/Fe^{3+}# ratio is sensitive to melt–rock reactions in mantle peridotites. Based on chromite data for 58 peridotites from oceanic and ophiolitic settings, Dare et al. (2009) proposed that the Ga–Ti–Fe^{3+}# systematics in chromite could be used to effectively discriminate peridotites from mid-ocean ridges (MORs) from those in SSZ settings. In a plot of Ga/Fe^{3+}# versus Ti/Fe^{3+}# (Fig. 9), chromites from the S16-TVG1 and S16-TVG5 serpentinized peridotites plot in the MOR residual to MOR reacted fields. Chromites in the S16-TVG4 samples plot in the SSZ reacted field toward

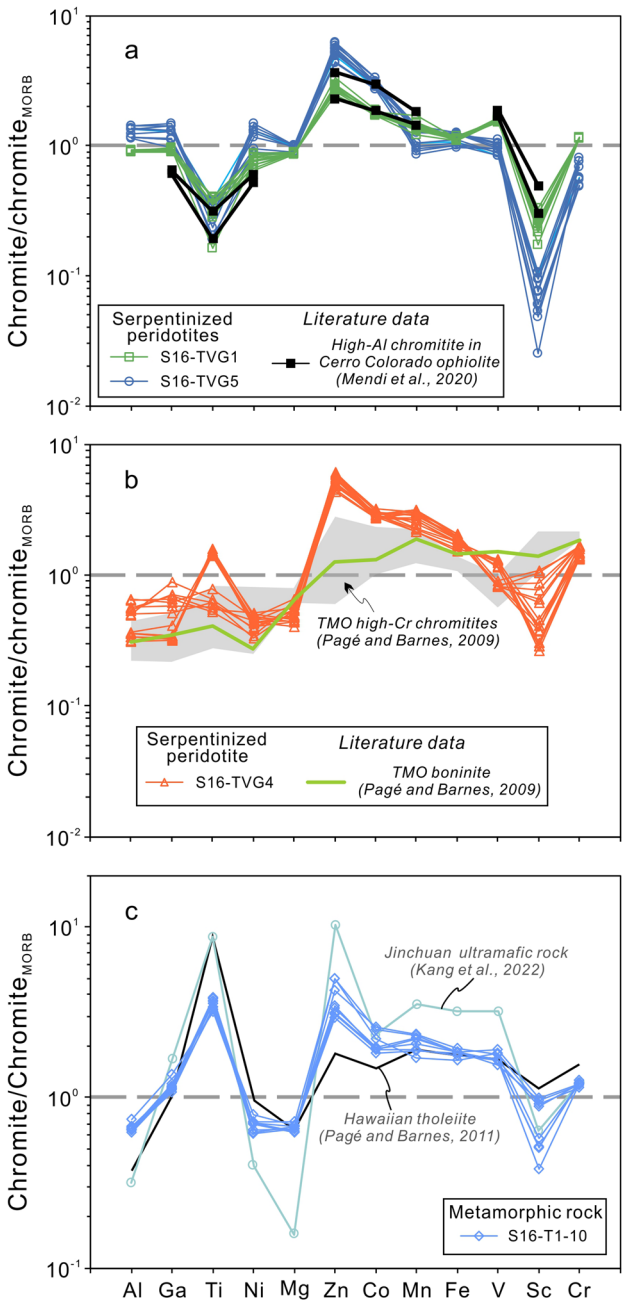

Fig. 8 MORB-normalized chromite major and trace element data for the serpentinized peridotites and metamorphic rock from the Yap–Mariana Junction. The MORB values are from Pagé and Barnes (2009). *TMO* Thetford Mines ophiolite

IAT melts. Chromites in the metamorphic rock plot in the MOR reacted field. In addition, some studies have documented that in mantle peridotites, the amphibole replacing clinopyroxene has high Cr_2O_3 contents, whereas magmatic amphibole crystalized from a hydrous melt has a pargasitic composition with low Cr_2O_3 contents (e.g., Gong et al. 2022; Sen et al. 2021). A few pargasitic amphiboles with low Cr_2O_3 contents were found in our peridotite samples

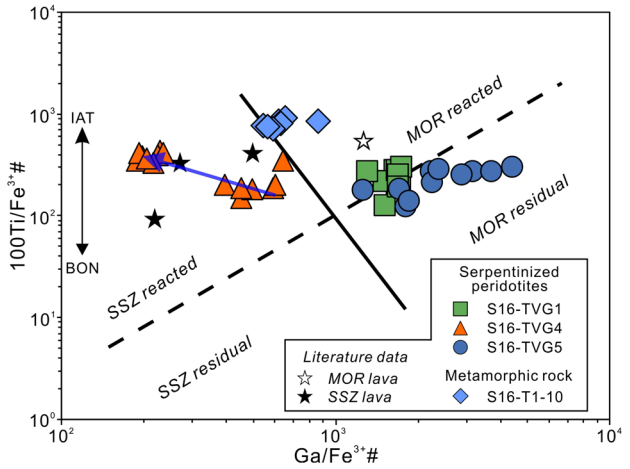

Fig. 9 Plot of chromite Ti/Fe^{3+}# versus Ga/Fe^{3+}# for the serpentinized peridotites and metamorphic rock from the Yap–Mariana Junction. The field boundaries and literature data are from Dare et al. (2009). *BON* boninite, *IAT* island arc tholeiite

(Figure S3c), possibly indicating the effects of water-rich melts percolating through the overlying mantle. The augitic clinopyroxene found in the metamorphic rock is common in mafic–ultramafic igneous rocks (e.g., Ohara et al. 2003), and contrasts with that in mantle peridotites (diopsidic clinopyroxene). Therefore, multiple lines of evidence indicate that the protoliths of the S16-TVG1 and S16-TVG5 serpentinized peridotites were derived from a MOR setting and are abyssal peridotites, whereas the S16-TVG4 samples are forearc peridotites formed in a SSZ setting. The protolith of the metamorphic rock is likely the crystallization product (i.e., a mafic–ultramafic rock) of a MORB-like melt.

Based on Fe–Mg exchange geothermobarometry using clinopyroxene–orthopyroxene, and Eqs. (37) and (38) of Putirka (2008), we estimated the equilibration temperature–pressure (*T*–*P*) of the protoliths of the S16-TVG1 and S16-TVG5 serpentinized peridotites. Because of the lack of primitive silicate mineral residuals (such as olivine and pyroxene) in the S16-TVG4 serpentinized peridotites, here we cannot estimate the T–P conditions of their protoliths. To minimize the effects of Cpx exsolution in orthopyroxene, the average compositions of Opx and Cpx in each sample and Opx–Cpx mineral pairs hosted in chromite were used in the calculations. The estimated *T*–*P* conditions of the protoliths are ~ 900 °C and ~ 4.6 kbar for the S16-TVG1 samples and 811–835 °C and 4.1–5.2 kbar for the S16-TVG5 samples (Table S6). A temperature range of 810–900 °C plots in the temperature field (740–900 °C based on major element-in-two-pyroxene thermometer; Dygert and Liang 2015) of mantle peridotites from supra-subduction zone (SSZ), but lower than that of abyssal peridotites (820–1180 °C). Based on thermometric data for mantle peridotites from SSZ and mid-ocean ridge (MOR) settings, Dygert and Liang (2015) proposed that the lower closure temperatures in SSZ ophiolites can result from the cooling over longer intervals relative to abyssal peridotites. Coincidentally, seismic tomography and receiver function analyses have revealed the subducted Caroline oceanic slab and oceanic plateau at depths of 60–350 km in the Yap subduction zone (Fan et al. 2022). The relatively low equilibration temperatures in group 1 peridotites could result from effect on thermal history of the overlying lithospheric mantle by the Caroline slab subduction.

Equilibrium melts of two groups of peridotites

The serpentinized peridotites from the Yap–Mariana Junction can be divided into two groups: group 1 abyssal peridotites (S16-TVG1 and S16-TVG5) and group 2 forearc peridotites (S16-TVG4). Because of the different formation settings, these two groups of mantle peridotites differ in terms of mineralogy and also partial melting. To further verify the tectonic settings and better understand the mantle evolution in this region, we estimated the composition of equilibrium melts with these protoliths, and compared these with volcanic rocks from various geological settings.

The empirical equations for Al_2O_3 and TiO_2 contents and FeO/MgO ratios have been established for chromite and equilibrium melt, which are independent of temperature (e.g., Kamenetsky et al. 2001; Maurel and Maurel 1982; Zaccarini et al. 2011). The equation for the FeO/MgO ratio of an equilibrium melt with chromite is as follows (Maurel and Maurel 1982):

$$\ln(\mathrm{FeO/MgO})_{\mathrm{Chr}} = 0.47 - 1.07 \times \mathrm{Al\#}_{\mathrm{Chr}} + 0.64 \times \mathrm{Fe\#}_{\mathrm{Chr}} + \ln(\mathrm{FeO/MgO})_{\mathrm{melt}},$$

where FeO and MgO are in wt.%, Al# = Al/(Cr + Al + Fe^{3+}) and Fe# = Fe^{3+}/(Cr + Al + Fe^{3+}). The equation for $(Al_2O_3)_{melt}$ in an arc setting is as follows (Zaccarini et al. 2011):

$$(Al_2O_3)_{melt} = 5.2253 \times \ln(Al_2O_3)_{Chr} - 1.1232.$$

The equations for $(TiO_2)_{melt}$ and $(Al_2O_3)_{melt}$ in a MORB setting are as follows (Zaccarini et al. 2011):

$$(TiO_2)_{melt} = 0.708 \times \ln(TiO_2)_{Chr} + 1.6436.$$

$$(Al_2O_3)_{melt} = 4.1386 \times \ln(Al_2O_3)_{Chr} + 2.2828,$$

where Al_2O_3 and TiO_2 are in wt%. To better depict the compositional difference in the equilibrium melts with the two groups of peridotites, we used the least-depleted S16-TVG5 samples (chromite Cr# = 0.15–0.29) to represent group 1, and the most-depleted S16-T4-M1-2 sample (chromite Cr# > 0.6) to represent group 2. According to the empirical formula [F = 0.1 × ln(Cr#) + 0.24; Hellebrand et al. 2001], the chromite Cr# values of the group 1 samples reflect low-degree melting (5.3%–11.5%; Fig. 10a). The calculated Mg# values [molar MgO/(FeO + MgO)] and Al_2O_3 contents of melts for group 1 are 0.52–0.62 and

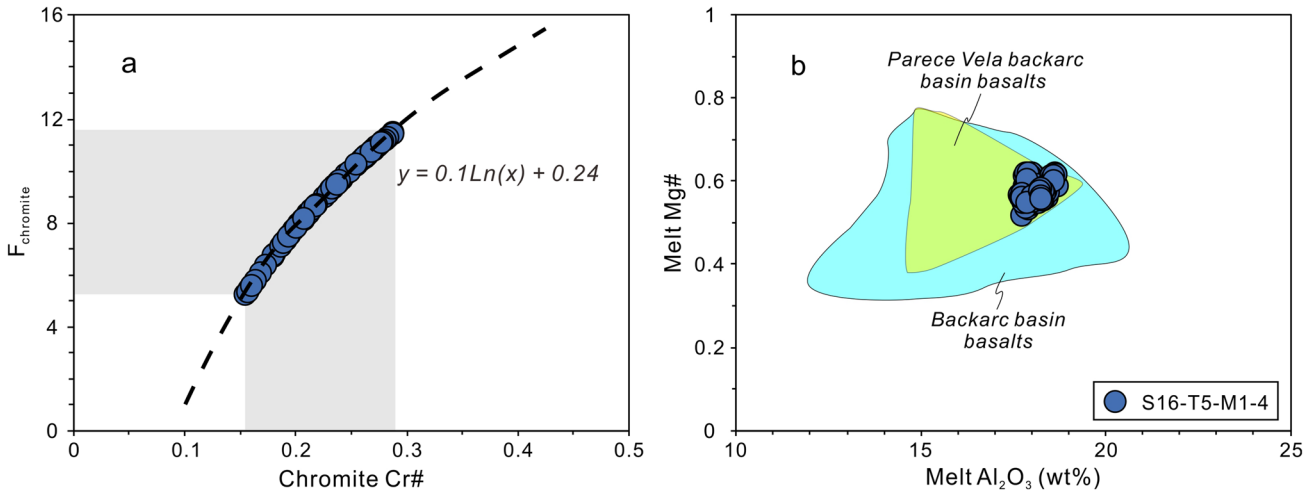

Fig. 10 **a** Calculated degree of melting of the protolith of sample S16-T5-M1-4 (group 1 abyssal peridotite). **b** Calculated Al_2O_3 and Mg# values of the melt in equilibrium with chromite as compared with back-arc basin basalts. Data for the back-arc basin and Parece Vela basalts are from the GEOROC database

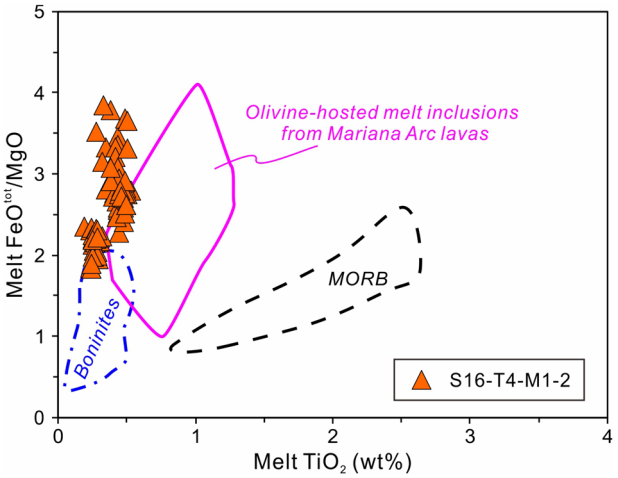

Fig. 11 Calculated TiO_2 and FeO^{tot}/MgO values of the melt in equilibrium with chromite from sample S16-T4-M1-2 (group 2 forearc peridotite) as compared with MORBs (Gale et al. 2013), boninites (GEOROC database), and olivine-hosted melt inclusions from the Mariana Arc (Kent and Elliott 2002; Lee and Stern 1998)

17.7–18.7 wt%, respectively, which plot in the field for PVB basalts (Fig. 10b). In contrast, the calculated TiO_2, Al_2O_3, and FeO/MgO values of melts for group 2 are 0.28–0.53 wt%, 11.9–13.8 wt%, and 2.28–3.85, respectively. The estimated melts for group 2 have higher FeO/MgO values than those of boninites, and lower TiO_2 contents than those of olivine-hosted melt inclusions from Mariana arc volcanic rocks, which are close to the trend for arc-related melts but far from the MORB trend (Fig. 11). Given that the sampling locations are close to the Parece Vela Rift, we suggest that the group 1 peridotites were derived from lithospheric mantle that experienced low-degree partial melting in a back-arc spreading ridge setting, whereas the group 2 samples were derived from a mantle wedge that experienced a second stage of partial melting in the Yap trench–arc system.

Melt percolation and reaction in the group 1 peridotites

Based on the LREE contents, two types of primary clinopyroxene (type 1 Cpx with low La/Sm and type 2 Cpx with high La/Sm ratios) were identified in the group 1 peridotites (Fig. 6). Type 1 Cpx with moderate depletions in LREEs has a similar REE composition as fertile peridotites in the Parece Vela Rift (Ohara et al. 2003). This type of Cpx is commonly thought to be a residual phase in abyssal peridotites after melt extraction at a slow-spreading ridge (Gong et al. 2022; Johnson et al. 1990; Sen et al. 2021). The relatively flat REE pattern of type 2 Cpx is consistent with those of plagioclase-bearing peridotites in the Parece Vela Rift (Ohara et al. 2003) and magmatic Cpx in some enriched basalts in the PVB (Yuan and Yan 2022). These two types of mantle Cpx have mainly been documented in melt-impregnated abyssal peridotites (Fig. 6b), such as amphibole-rich peridotites from the Mado Megamullion, Shikoku Basin (Sen et al. 2021), and peridotites from the Mariana Trough (Ohara et al. 2002b) and Parece Vela Rift (Gong et al. 2022). Because partial melting decreases the LREE contents of mantle clinopyroxene and cannot generate the REE patterns of type 2 Cpx, we suggest that type 2 Cpx was produced by reactions between mantle Cpx and LREE-enriched melts, or that it crystallized from LREE-enriched melts. Therefore, the two types of Cpx in the group 1 peridotites record partial

melting and melt–rock reactions in the mantle beneath the Yap–Mariana Junction.

To better constrain these processes, we first used simple models of equilibrium melting (Shaw 1970) and fractional melting (Johnson et al. 1990) to reproduce the REE contents of type 1 Cpx. In the modeling, a whole-rock composition (major elements and REEs) of a spinel peridotite from Workman and Hart (2005) was used as the starting composition. The initial mineral mode and melting mode used in the models are listed in Table S7. The partition coefficients between melt and olivine, clinopyroxene, orthopyroxene, and spinel are listed in Table S8. As shown in Fig. 6a, both ~ 15% batch melting and ~ 5% fractional melting of depleted MORB mantle can reproduce the REE contents of the type 1 Cpx, except for the La–Ce enrichment that is common in ocean floor peridotites (Johnson et al. 1990; Ohara et al. 2002b). The fractional melting model is more consistent with the 5.3%–11.5% melting estimated from the chromite Cr# values of the S16-TVG5 samples. The presence of two types of Cpx and the Cpx–Opx inclusions in the chromite indicates open-system behavior in the mantle. Therefore, we used an open-system model (Ozawa and Shimizu 1995) to model the REE patterns of type 1 Cpx. We assumed that the influxing material was enriched melt in equilibrium with type 2 Cpx, and its REE contents are listed in Table S8. An open-system model that has ~ 0.6 wt.% of interstitial melt ($\alpha = 0.006$; α refers to ratio of trapped melt mass against residual solid mass), a mass influx rate of 0.01 ($\beta = 0.01$; β refers to influxing mass fraction of the initial solid mass divided by degree of melting), and 6% partial melting ($F = 0.06$) can reproduce the observed REE patterns of type 1 Cpx. The negative Eu anomaly in the type 2 Cpx commonly occurs in the melt-impregnated mantle peridotite samples (Fig. 6a), such as the Parece Vela Rift (Ohara et al. 2003), the Parece Vela back-arc (Gong et al. 2022) and the Mado Megamullion in Shikoku Basin (Sen et al. 2021). Additionally, though no any pyroxene residual is persevered in the S16-TVG1 peridotites, the slightly elevated Cr# and TiO_2 values in chromites also plot within the trend of harzburgite-MORB-like melt reaction (Fig. 3d). These evidences confirm that melt impregnation and melt–rock reactions occurred in the upper mantle beneath the Yap–Mariana Junction.

Implications for the role of ultra-slow subduction in a magma-starved arc

Dating of the Yap amphibolites has revealed that the collision between the Caroline Ridge and Yap Trench occurred at *ca*. 21 Ma (Zhang and Zhang 2020). After the collision, the convergence rate along the Yap Trench decreased to 0–6 mm/yr (Seno et al. 1993). If we assume a subduction rate of 6 mm/yr, then ~ 120 km of subduction would have occurred since 21 Ma. Recent P-wave tomographic results have shown that the Caroline oceanic slab has subducted down to depths of 60–350 km to the north of Yap Island (Fan et al. 2022). This implies that the Caroline slab has subducted to the depth of the sub-arc mantle region that generally would produce a large amount of arc magmatism (e.g., the typical IBM trench–arc system; Stern et al. 2003). However, only short-lived arc volcanism at 11–7 Ma occurred in the Yap Trench, which is considered to have been related to subduction in the Sorol Trough (Crawford et al. 1986) or the breakoff of subducted slab (Fan et al. 2022). The reason for the paucity of volcanic rocks in the Yap arc system remains poorly understood.

Previous studies (Okino et al. 1998; Ohara et al. 2001; Tani et al. 2011) demonstrated the spreading of the Parece Vela Basin was from ~ 29–7.9 Ma. The Caroline Ridge touched with Yap Trench at ~ 21 Ma and subsequently continued to subduct. Geophysical researches (e.g., Fan et al. 2022) also revealed the presence of the Caroline oceanic slab in the deep mantle. Namely, this region underwent a tectonic transition from a back-arc spreading ridge to a subduction zone. In this study, we discovered abyssal peridotites (group 1; S16-TVG1 and S16-TVG5 samples), forearc peridotites (group 2; S16-TVG4 samples), and a greenschist (S16-T1-10) at the Yap–Mariana Junction, which have a wide range of geochemical compositions. Likewise, this finding provides a new geochemical record that evidences such a tectonic transformation. The S16-TVG5 peridotites exhibit several geochemical features typical of low-degree mantle melting, such as high whole-rock CaO (up to 3.93 wt%), Al_2O_3 (up to 2.98 wt%), and Al_2O_3/SiO_2 (up to 0.07) values, low chromite Cr# values (as low as 0.16), and intermediate LREE contents in the type 1 Cpx (6% open-system melting). However, previous studies (Ohara et al. 2001, 2003) have shown that the PVB spreading ridge had a relatively high spreading rate (7.0–8.8 cm/yr), which appears to be incompatible with low-degree mantle melting. The unusual mullion structures that commonly develop at slow-spreading ridges (e.g., the Mid-Atlantic Ridge megamullions; Tucholke et al. 1998) are also found along the Parece Vela Rift (Ohara et al. 2001). Ohara et al. (2003) suggested that the origins of fertile peridotites in the Parece Vela Rift were related to extreme transform faults that result from the ridge-transform geometry of short first-order segments (i.e., the formation of mullions). The formation of prominent fracture zones occurred after the counter-clockwise rotation of the spreading axes from N–S to NW–SE at *ca.* 19 Ma. Therefore, we suggest that the group 1 peridotites were also produced by low-degree mantle melting in the Parece Vela Rift during the formation of the mullion structures. Subsequently, these mantle peridotites experienced MORB-like melt impregnation and melt–rock reactions, indicated by geochemical features of chromites and two types of Cpx. Given that the group 2 peridotites have similar compositional features to forearc

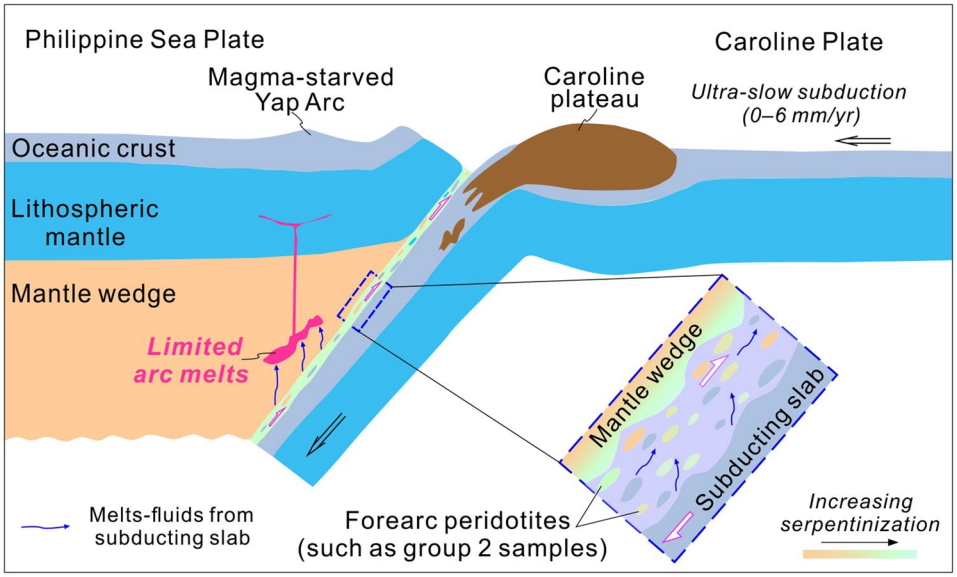

Fig. 12 Conceptual model for the magma-starved Yap Arc and ultra-slow subduction of the Caroline Plateau

setting, therefore, we propose that this region subsequently experienced a second mantle wedge melting event during subduction of the Caroline Plateau, but few arc melts were erupted. Moreover, though an origin of reactive dunites in an arc setting cannot be completely ruled out, four lines of evidence support that the group 2 peridotites were more likely derived from the overlying residual mantle wedge that experienced the partial melting. (1) These samples were collected by TV-guided grab (TVG) at the Yap Trench, and only small amount of arc melts were produced in this subduction system. (2) The reactive dunites commonly contain silicate inclusions (e.g., pyroxene and amphibole) hosted in chromite, which are not observed in group 1 samples. (3) In the group 2 peridotites, the occurrence of pargasites formed in high T–P conditions indicates that they could derive from deep mantle. (4) Other than mantle peridotites, metamorphic rocks were also collected in these assignments. The presence of these metamorphic rocks indicates the Yap Trench has developed a subduction channel and may have experienced the exhumation of subducting components.

Incipient plateau subduction in other regions has also dramatically decreased the subduction rate and suppressed or stopped arc volcanism (e.g., McGeary et al. 1985; van Hunen et al. 2002). The explanations for such a volcanic gap include: (1) the absence of a favorable stress state in the overlying lithosphere; and (2) the lack of a mantle wedge that generates the magmatism. The former hinders the differentiation of arc basaltic magmas and prevents the formation of andesitic arc volcanoes, whereas the latter mainly results in a decreased melt flux (McGeary et al. 1985). In contrast to the intermediate convergence rate of 3–6 cm/yr in the Mariana Trench (Stern et al. 2003), the ultra-low subduction rate (0–6 mm/yr) of the Caroline Plateau reduces the supply of volatiles and melts from the subducting slab to the mantle wedge, which greatly reduces the amount of arc magmatism. Compared with the Mariana Forearc peridotites (normal oceanic crustal subduction), the group 2 forearc peridotites (oceanic plateau subduction) from the Yap Trench show relatively higher whole-rock Al_2O_3/SiO_2 ratios, higher whole-rock contents of heavy rare earth elements (HREE), and moderate Cr# values in chromite. These geochemical features may indicate that they are compositionally less depleted. We now propose a model for the magma-starved Yap Arc (Fig. 12). Due to ultra-slow subduction of the Caroline Plateau in the Yap subduction zone, the mantle wedge was metasomatized by a small amount of slab-derived melts and fluids, and may undergo a relatively lower melting degree than the Mariana trench–arc system. Limited arc melts derived from the mantle wedge did not pass through the lithosphere, resulting in an absence of arc volcanic rocks. Therefore, we suggest that the group 2 forearc peridotites are part of an overlying new mantle wedge that formed during subduction of the Caroline Plateau, and that a limited supply of arc melts was the key factor in the formation of the magma-starved Yap Arc.

Conclusion

The Yap trench–arc system is undergoing subduction of an oceanic plateau and provides a rare opportunity to investigate such subduction processes. We investigated the mineralogy and geochemistry of serpentinized peridotites from the Yap–Mariana Junction and mainly reached the following conclusions.

(1) Based on the geochemical compositions of the whole-rock samples and minerals, two different protoliths were identified for the serpentinized peridotites: group 1 abyssal peridotites (S16-TVG1 and S16-TVG5) and group 2 forearc peridotites (S16-TVG4).

(2) Two types of clinopyroxene are found in the group 1 abyssal peridotites. REE patterns of type 1 Cpx (low La/Sm ratios) can be reproduced by ~ 5% fractional melting or ~ 6% open-system melting of depleted MORB mantle, whereas type 2 Cpx (high La/Sm ratios) is related to LREE-enriched melts, implying that melt impregnation and reactions occurred in the upper mantle beneath the Yap–Mariana Junction.

(3) The two groups of peridotites from the Yap–Mariana Junction record a tectonic transition from a back-arc spreading ridge to oceanic plateau subduction.

(4) Compared with the Mariana Trench, the absence of arc volcanic rocks at the Yap Trench reflects the limited development of a mantle wedge due to ultra-slow subduction of the Caroline Plateau.

Supplementary Information The online version contains supplementary material available at https://doi.org/10.1007/s00410-023-02056-2.

Acknowledgements We gratefully acknowledge Véronique Le Roux and one anonymous reviewer for their constructive comments and suggestions, and Editor Timm John for the constructive comments and efficient editorial handling. All these comments significantly improved the manuscript. Samples were collected onboard R/V "KE XUE" implementing the open research cruise NORC2020-581 supported by NSFC Shiptime Sharing Project. We thank Shuai Wang for EMPA mineral major oxide analyses. This work was supported by the Strategic Priority Research Program of the Chinese Academy of Sciences (XDB42020302), the National Natural Science Foundation of China (91858206, 42221005, 42206051), Marine S&T Fund of Shandong Province for Pilot National Laboratory for Marine Science and Technology (Qingdao) (Grant No. 2022QNLM050201-3), Natural Science Foundation of Shandong Province (ZR2020MD070, ZR2022QD027), and Taishan Scholars Program of Shandong Province (tsqn201909157).

Data availability All data in this study are available in the supplementary materials.

References

Arai S (1994) Characterization of spinel peridotites by olivine-spinel compositional relationships: review and interpretation. Chem Geol 113(3–4):191–204

Beccaluva L, Serri G, Dostal J (1986) Geochemistry of volcanic rocks from the mariana, yap and palau trenches bearing on the tectono-magmatic evolution of the mariana trench-arc-backarc system. Developments in geotectonics, vol 21. Elsevier, pp 481–508

Birner SK, Warren JM, Cottrell E, Davis FA, Kelley KA, Falloon TJ (2017) Forearc peridotites from tonga record heterogeneous oxidation of the mantle following subduction initiation. J Petrol 58(9):1755–1780

Boynton WV (1984) Cosmochemistry of the rare earth elements: meteorite studies. Developments in geochemistry, vol 2. Elsevier, pp 63–114

Chen L, Tang L, Li X, Dong Y, Yu X, Ding W (2019a) Geochemistry of peridotites from the yap trench, Western Pacific: implications for subduction zone mantle evolution. Int Geol Rev 61(9):1037–1051

Chen L, Tang L, Li X, Zhang J, Wang W, Li Z, Wang H, Wu X, Chu F (2019b) Ancient melt depletion and metasomatic history of the subduction zone mantle: osmium isotope evidence of peridotites from the Yap Trench. West Pac Minerals 9(12):717

Cloos M (1993) Lithospheric buoyancy and collisional orogenesis: subduction of oceanic plateaus, continental margins, Isl Arcs, spreading ridges, and seamounts. Geol Soc Am Bull 105(6):715–737

Crawford A, Beccaluva L, Serri G, Dostal J (1986) Petrology, geochemistry and tectonic implications of volcanics dredged from the intersection of the yap and mariana trenches. Earth Planet Sci Lett 80(3–4):265–280

Dare SA, Pearce JA, McDonald I, Styles MT (2009) Tectonic discrimination of peridotites using fO_2–Cr# and Ga–Ti–Fe^{III} systematics in chrome–spinel. Chem Geol 261(3–4):199–216

Dick HJ, Bullen T (1984) Chromian spinel as a petrogenetic indicator in abyssal and alpine-type peridotites and spatially associated lavas. Contrib Mineral Petrol 86(1):54–76

Doley B, Saha A, Verencar A, Mohan MR (2022) Melt generation and trace element fractionation of intermediate arc magma from Andaman subduction zone. Geochemistry 82(3):125899

Dong D, Zhang Z, Bai Y, Fan J, Zhang G (2018) Topographic and sedimentary features in the yap subduction zone and their implications for the caroline ridge subduction. Tectonophysics 722:410–421

Dygert N, Liang Y (2015) Temperatures and cooling rates recorded in REE in coexisting pyroxenes in ophiolitic and abyssal peridotites. Earth Planet Sci Lett 420:151–161

Fan J, Zheng H, Zhao D, Dong D, Bai Y, Li C, Zhang Z (2022) Seismic structure of the caroline plateau-yap trench collision zone. Geophys Res Lett 49(6):e2022GL098017

Fujiwara T, Tamura C, Nishizawa A, Fujioka K, Kobayashi K, Iwabuchi Y (2000) Morphology and tectonics of the yap trench. Mar Geophys Res 21(1):69–86

Gale A, Dalton CA, Langmuir CH, Su Y, Schilling JG (2013) The mean composition of ocean ridge basalts. Geochem Geophy Geosy 14(3):489–518

Gong X, Tian L, Dong Y (2022) Contrasting melt percolation and melt-rock reactions in the parece vela back-arc oceanic lithosphere. Philipp Sea: A Mineral Perspect Lithos 422:106727

Gorczyk W, Willner AP, Gerya TV, Connolly JA, Burg J-P (2007) Physical controls of magmatic productivity at Pacific-type convergent margins: numerical modelling. Phys Earth Planet Inter 163(1–4):209–232

Hawkins J, Batiza R (1977) Metamorphic rocks of the Yap arc-trench system. Earth Planet Sci Lett 37(2):216–229

Hawkins JW, Bloomer SH, Evans CA, Melchior JT (1984) Evolution of intra-oceanic arc-trench systems. Tectonophysics 102(1–4):175–205

Hellebrand E, Snow JE, Dick HJ, Hofmann AW (2001) Coupled major and trace elements as indicators of the extent of melting in mid-ocean-ridge peridotites. Nature 410(6829):677–681

Holt AF, Condit CB (2021) Slab temperature evolution over the lifetime of a subduction zone. Geochem Geophy Geosy 22(6):e2020GC009476

Jagoutz E, Palme H, Baddenhausen H, Blum K, Cendales M, Dreibus G, Spettel B, Lorenz V, Wänke H (1979) The abundances of major, minor and trace elements in the earth's mantle as derived from primitive ultramafic nodules. Lunar and Proc Lunar Planet Sci Conf 10:2031–2050

Johnson KT, Dick HJ, Shimizu N (1990) Melting in the oceanic upper mantle: an ion microprobe study of diopsides in abyssal peridotites. J Geophys Res 95(B3):2661–2678

Kamenetsky VS, Crawford AJ, Meffre S (2001) Factors controlling chemistry of magmatic spinel: an empirical study of associated

olivine, Cr-spinel and melt inclusions from primitive rocks. J Petrol 42(4):655–671
Kang J, Chen L-M, Yu S-Y, Zheng W-Q, Dai Z-H, Zhou S-H, Ai Q-X (2022) Chromite geochemistry of the Jinchuan Ni-Cu sulfide-bearing ultramafic intrusion (NW China) and its petrogenetic implications. Ore Geol Rev 141:104644
Karig DE (1971) Structural history of the mariana Isl Arc system. Geol Soc Am Bull 82(2):323–344
Kent AJ, Elliott TR (2002) Melt inclusions from Marianas arc lavas: implications for the composition and formation of Isl Arc magmas. Chem Geol 183(1–4):263–286
Kerr AC, Mahoney JJ (2007) Oceanic plateaus: Problematic plumes, potential paradigms. Chem Geol 241(3–4):332–353
Knesel KM, Cohen BE, Vasconcelos PM, Thiede DS (2008) Rapid change in drift of the Australian plate records collision with ontong java plateau. Nature 454(7205):754–757
Kobayashi K (2004) Origin of the palau and Yap trench-arc systems. Geophys J Int 157(3):1303–1315
Lee J, Stern RJ (1998) Glass inclusions in Mariana Arc phenocrysts: a new perspective on magmatic evolution in a typical intra-oceanic arc. J Geol 106(1):19–34
Liu Y, Hu Z, Gao S, Günther D, Xu J, Gao C, Chen H (2008) In situ analysis of major and trace elements of anhydrous minerals by LA-ICP-MS without applying an internal standard. Chem Geol 257(1–2):34–43
Liu Z, Dai L, Li S, Wang L, Xing H, Liu Y, Ma F, Dong H, Li F (2021) When plateau meets subduction zone: a review of numerical models. Earth-Sci Rev 215:103556
Loocke M, Snow JE, Ohara Y (2013) Melt stagnation in peridotites from the godzilla megamullion oceanic core complex, parece vela basin, Philippine sea. Lithos 182:1–10
Maurel C, Maurel P (1982) Étude expérimental de la distribution de l'aluminium entre bain silicate basique et spinelle chromifère. Implications pétrogenetiques: teneur en chrome des spinelles. Bulletin de Mineralogie 105:197–202
McGeary S, Nur A, Ben-Avraham Z (1985) Spatial gaps in arc volcanism: the effect of collision or subduction of oceanic plateaus. Tectonophysics 119(1–4):195–221
Mendi DJ, González-Jiménez JM, Proenza JA, Urbani F, Gervilla F (2020) Petrogenesis of the chromitite body from the cerro colorado ophiolite, paraguaná peninsula. Venezuela Bol Soc Geol Mex 72(3):27
Michibayashi K, Ohara Y, Stern R, Fryer P, Kimura JI, Tasaka M, Harigane Y, Ishii T (2009) Peridotites from a ductile shear zone within back-arc lithospheric mantle, southern Mariana trench: results of a shinkai 6500 dive. Geochem Geophy Geosy. https://doi.org/10.1029/2008GC002197
Murata K, Maekawa H, Yokose H, Yamamoto K, Fujioka K, Ishii T, Chiba H, Wada Y (2009) Significance of serpentinization of wedge mantle peridotites beneath Mariana forearc, western Pacific. Geosphere 5(2):90–104
Nair R, Chacko T (2008) Role of oceanic plateaus in the initiation of subduction and origin of continental crust. Geology 36(7):583–586
Niu Y (1997) Mantle melting and melt extraction processes beneath ocean ridges: evidence from abyssal peridotites. J Petrol 38(8):1047–1074
Niu Y (2004) Bulk-rock major and trace element compositions of abyssal peridotites: implications for mantle melting, melt extraction and post-melting processes beneath mid-ocean ridges. J Petrol 45(12):2423–2458
Ohara Y, Ishii T (1998) Peridotites from the southern Mariana forearc: heterogeneous fluid supply in mantle wedge. Isl Arc 7(3):541–558
Ohara Y, Yoshida T, Kato Y, Kasuga S (2001) Giant megamullion in the parece vela backarc basin. Mar Geophys Res 22(1):47–61
Ohara Y, Fujioka K, Ishizuka O, Ishii T (2002a) Peridotites and volcanics from the Yap arc system: implications for tectonics of the southern Philippine sea plate. Chem Geol 189(1–2):35–53
Ohara Y, Stern RJ, Ishii T, Yurimoto H, Yamazaki T (2002b) Peridotites from the Mariana trough: first look at the mantle beneath an active back-arc basin. Contrib Mineral Petrol 143(1):1–18
Ohara Y, Fujioka K, Ishii T, Yurimoto H (2003) Peridotites and gabbros from the parece vela backarc basin: unique tectonic window in an extinct backarc spreading ridge. Geochem Geophy Geosy 4(7):8611. https://doi.org/10.1029/2002GC000469
Okamura H, Arai S, Kim Y-U (2006) Petrology of forearc peridotite from the Hahajima Seamount, the Izu-Bonin arc, with special reference to chemical characteristics of chromian spinel. Mineral Mag 70(1):15–26
Okino K, Kasuga S, Ohara Y (1998) A new scenario of the parece vela basin genesis. Mar Geophys Res 20(1):21–40
Ozawa K, Shimizu N (1995) Open-system melting in the upper mantle: constraints from the Hayachine-Miyamori ophiolite, northeastern Japan. J Geophys Res 100(B11):22315–22335
Pagé P, Barnes S-J (2009) Using trace elements in chromites to constrain the origin of podiform chromitites in the thetford mines ophiolite, Québec. Canada Econ Geol 104(7):997–1018
Pagé P, Barnes S-J, Zientek ML (2011) Formation and evolution of the chromitites of the stillwater complex: a trace element study. In: Barra F (ed) Let's talk ore deposits: proceedings of the 11th SGA Biennial Meeting, Antofagasta, Chile. Society for Geology Applied to Mineral Deposits, pp 678–680
Palme H, O'Neill HSC (2003) 3.1 Cosmochemical estimates of mantle composition. Treatise Geochem 2:1–38
Parkinson IJ, Pearce JA (1998) Peridotites from the Izu–Bonin–Mariana forearc (ODP Leg 125): evidence for mantle melting and melt–mantle interaction in a supra-subduction zone setting. J Petrol 39(9):1577–1618
Putirka KD (2008) Thermometers and barometers for volcanic systems. Rev Mineral Geochem 69(1):61–120
Reagan MK, Ishizuka O, Stern RJ, Kelley KA, Ohara Y, Blichert-Toft J, Bloomer SH, Cash J, Fryer P, Hanan BB (2010) Fore-arc basalts and subduction initiation in the Izu-Bonin-Mariana system. Geochem Geophy Geosy. https://doi.org/10.1029/2009GC002871
Rosenbaum G, Giles D, Saxon M, Betts PG, Weinberg RF, Duboz C (2005) Subduction of the nazca ridge and the inca plateau: insights into the formation of ore deposits in Peru. Earth Planet Sci Lett 239(1–2):18–32
Royden LH, Husson L (2009) Subduction with variations in slab buoyancy: models and application to the banda and apennine systems. Subduction zone geodynamics. Springer, pp 35–45
Saboda K, Fryer P, Maekawa H (1992) Metamorphism of ultramafic clasts from conical seamount: Sites 778, 779, and 780. Proc Ocean Drill Program Sci Results 125:431–443
Sato T, Kasahara J, Katao H, Tomiyama N, Mochizuki K, Koresawa S (1997) Seismic observations at the Yap Islands and the northern Yap trench. Tectonophysics 271(3–4):285–294
Schellart WP (2005) Influence of the subducting plate velocity on the geometry of the slab and migration of the subduction hinge. Earth Planet Sci Lett 231(3–4):197–219
Sen A, Snow J, Ohara Y, Hirauchi K, Kouketsu Y, Sanfilippo A, Basch V, Harigane Y, Fujii M, Okino K (2021) Melting and evolution of amphibole-rich back-arc abyssal peridotites at the mado megamullion Shikoku Basin. Geochem Geophy Geosy 22(12):e2021GC010013
Seno T, Stein S, Gripp AE (1993) A model for the motion of the Philippine sea plate consistent with NUVEL-1 and geological data. J Geophys Res 98(B10):17941–17948
Shaw DM (1970) Trace element fractionation during anatexis. Geochim Cosmochim Acta 34(2):237–243

Snow JE, Dick HJ (1995) Pervasive magnesium loss by marine weathering of peridotite. Geochim Cosmochim Acta 59(20):4219–4235
Standish J, Hart S, Blusztajn J, Dick H, Lee K (2002) Abyssal peridotite osmium isotopic compositions from cr-spinel. Geochem Geophy Geosy 3(1):1–24
Stern RJ, Fouch MJ, Klemperer SL (2003) An overview of the Izu-Bonin-Mariana subduction factory. In: Eiler J, Hirschmann M (eds) Inside the subduction factory, vol 138. AGU Monograph, Washington DC, pp 175–222
Tamura A, Arai S (2006) Harzburgite–dunite–orthopyroxenite suite as a record of supra-subduction zone setting for the Oman ophiolite mantle. Lithos 90(1–2):43–56
Tani K, Dunkley DJ, Ohara Y (2011) Termination of backarc spreading: zircon dating of a giant oceanic core complex. Geology 39(1):47–50
Tucholke BE, Lin J, Kleinrock MC (1998) Megamullions and mullion structure defining oceanic metamorphic core complexes on the Mid-Atlantic ridge. J Geophys Res 103(B5):9857–9866
Turner S, Bourdon B, Hawkesworth C, Evans P (2000) ^{226}Ra–^{230}Th evidence for multiple dehydration events, rapid melt ascent and the time scales of differentiation beneath the tonga-kermadec Isl Arc. Earth Planet Sci Lett 179(3–4):581–593
Van Hunen J, Van Den Berg AP, Vlaar NJ (2002) On the role of subducting oceanic plateaus in the development of shallow flat subduction. Tectonophysics 352(3–4):317–333
Wark D, Kempter K, McDowell F (1990) Evolution of waning, subduction-related magmatism, northern sierra madre occidental. Mexico Geol Soc Am Bull 102(11):1555–1564
Warren JM (2016) Global variations in abyssal peridotite compositions. Lithos 248:193–219
Wei SS, Shearer PM, Lithgow-Bertelloni C, Stixrude L, Tian D (2020) Oceanic plateau of the Hawaiian mantle plume head subducted to the uppermost lower mantle. Science 370(6519):983–987
Workman RK, Hart SR (2005) Major and trace element composition of the depleted MORB mantle (DMM). Earth Planet Sci Lett 231(1–2):53–72
Yao J-H, Zhu W-G, Li C, Zhong H, Bai Z-J, Ripley EM, Li C (2018) Petrogenesis and ore genesis of the Lengshuiqing magmatic sulfide deposit in southwest China: constraints from chalcophile elements (PGE, Se) and Sr-Nd-Os-S isotopes. Econ Geol 113(3):675–698
Yao J-H, Zhu W-G, Li C, Zhong H, Yu S, Ripley EM, Bai Z-J (2019) Olivine O isotope and trace element constraints on source variation of picrites in the emeishan flood basalt province, SW China. Lithos 338:87–98
Yao J, Xu J, Wu C, Zhang Z, Rosana MF, Li X, Jin Z (2023) Origin of high-Cr podiform chromitites from Kabaena Island, Southeast Sulawesi, Indonesia: constraints from mineralogy and geochemistry. Int Geol Rev. https://doi.org/10.1080/00206814.2023.2167130
Yuan L, Yan Q (2022) Source lithology and magmatic processes recorded in the mineral of basalts from the parece vela basin. Acta Geol Sin-Engl. https://doi.org/10.1111/1755-6724.14937
Zaccarini F, Garuti G, Proenza JA, Campos L, Thalhammer OA, Aiglsperger T, Lewis JF (2011) Chromite and platinum group elements mineralization in the santa elena ultramafic nappe (costa rica): geodynamic implications. Geol Acta 9(3–4):407–423
Zanetti A, D'Antonio M, Spadea P, Raffone N, Vannucci R, Bruguier O (2006) Petrogenesis of mantle peridotites from the Izu-Bonin-Mariana (IBM) forearc. Ofioliti 31(2):189–206
Zhang J, Zhang G (2020) Geochemical and chronological evidence for collision of proto-Yap arc/Caroline plateau and rejuvenated plate subduction at Yap trench. Lithos 370:105616
Zhang G, Zhang J, Wang S, Zhao J (2020) Geochemical and chronological constraints on the mantle plume origin of the Caroline Plateau. Chem Geol 540:119566